



---

**AXIAL DENSITY PROFILE OF 27 MHZ CAPACITIVELY COUPLED RF PLASMA;  
POWER AND PRESSURE DEPENDENCE**

**S. Helhel<sup>1,2</sup>**

<sup>1</sup> Akdeniz University, Engineering Faculty,  
Electrical and Electronics Engineering, Antalya, Turkey  
<sup>2</sup> KEYTEK Electrical and Electronics Ltd. Coop., Antalya

Accepted Date: 05 July 2009

**Abstract**

*Axial density profiles of Confined Capacitively Coupled Plasma (CCCP) are measured for different pressure and power levels with a microwave interferometer. Abel inversion is used to deduce radial density profiles, which show that density diffuses from center to the quartz tube walls and indicate different density profiles depending on the pressure and power. The preheat like potential drop from center to close to the boundary edge is approximately twice the electron temperature, while the density drops approximately five to eight times.*

**Keywords:** Plasma density, Microwave interferometer, Confined Capacitively Coupled Plasma, Pre-sheath.

**1. Introduction**

Plasma density and density distribution are crucial parameters in several applications such as semiconductor [1] and flat panel display [2] manufacturing, and plasma enhanced chemical reactions such as polymer modification [3]. Capacitively coupled plasma sources are widely used in semiconductor manufacturing and recent trends are to operate at higher densities and lower pressures in order to obtain higher etch rates and better ion anisotropy at the substrates [4]. For ion driven surface chemistry, knowing the radial plasma density profile is an important parameter as it directly relates to uniformity. Many plasma applications require knowing an axial or longitudinal local plasma number density distribution. This local plasma density distribution estimation can be achieved by computational modeling of plasma system responses under different conditions.

Microwave interferometer (MWI) is a well established, non-invasive technique for measurement of the line integrated plasma density, yielding the average density across a chord of the plasma. MWI line integral density measurements have also been used to calibrate Langmuir probes [5,6]. Using a collection of measurements from different chords of the plasma, Abel inversion can be employed to determine the radial plasma density profile. These line integrals are reduced to the first kind integral equation, and in the case of axi-symmetric two-dimensional plane, observation paths are parallel to each other which defines the problem as 'symmetric' Abel inversion [7]. Many other extensions, defined as asymmetric Abel inversion, have been developed for non-parallel observation paths, but these are beyond the scope of our work. Many different techniques for performing the numeric of the Abel inversion have been developed including neural networks[7], Legendre polynomials [8], fitting to high-order polynomials [9],

and in this work we employ a technique based on Fourier-Bessel function expansions [10]. The Fourier-Bessel approach has an advantage in the case of where the system does not allow us parallel chord measurements, and the solution is less sensitive to random errors occurred during the measurements, and it is a robust system for the application to experimental data.

Lukas et al [11] studied the electron distribution in the argon plasma of a Capacitively coupled parallel plate reactor frequency of 13.56 MHz. Lukas et al [11] made a line-of-sight integrated electron density measurement by using a 1 mm interferometer, and formulated them by using Abel inversion. Lukas et al proposed that their results are similar like model responses. Lukas et al noted that in order to obtain reliable results from the Abel inversion procedure, it is necessary to measure line-of-sight integrated phase shifts also for chords extending through the far edge of the rotationally symmetric plasma.

The physical properties of our heterodyne interferometer have been explained in an earlier publication [12] and have been communicated with first measurements on a confined RF discharge. On the basis of Abel inversion formulation, radial electron density profile is contributed by this paper. Fourier-Bessel function expansion is described in section two, plasma chamber and MWI system are briefly described in section three and in section four radial electron number density distribution variations as a function of pressure and applied power for 27.12 MHz C-CCP plasma chamber are given and discussed.

## 2. Theory

Symmetric Abel inversion can be performed to give radial density profiles from chord-averaged densities. Figure 1 shows a cross-section of the cylindrical plasma showing one chord labeled as 'L'. The position of the chord is defined by the minimum radii 'r'.

In our experiment we have 5 chords measured at  $r=[0,1,2,3,4 \text{ cm}]$ , further measurement points were not in our measurement capabilities because of our interferometer operating frequency.

$$I(p,j) = \int_L n(r,q) dS \quad (1)$$

where:  $n(r,\theta)$  is the local plasma density at polar coordinates of  $r$  and  $\theta$ , and  $I(p,j)$  is the integrated value of density along the observation path  $L$ , a function of pressure and RF power. Mathematically, the function  $n(r,\theta)$  can be expanded in terms of  $r$  and  $\theta$  assuming that density distribution is symmetric [4], as in Equation 2.

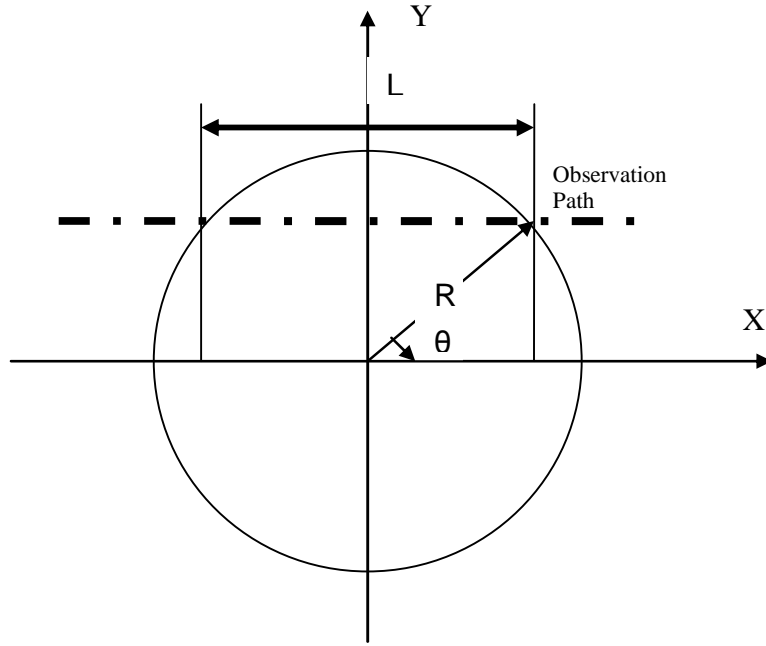


Fig. 1 Geometry of the Coordinate System.

$$n(r, q) = \sum_{m=0}^{\infty} \sum_{l=0}^{\infty} [a_m^l \cos(mq)] g_m'(r) \quad (2)$$

$$I(p, j) = \sum_{m=0}^{\infty} \sum_{l=0}^{\infty} \left[ a_m^l \int_L (\cos(q)) g_m'(r) dS \right] \quad (3)$$

The coefficients are found by least-square fit of equation 3 to measured data. Instead above equation can be expanded in several form of r, the first kind Bessel expansion of above equation has been chosen as Roan et al [10].

$$g_m'(r) = J_m(I_m^{l+1} r) \quad (4)$$

We made only a single array line integral measurements that requires only the term m=0 is left, and to obtain the best results we need to choose 8 measurement values for Equation 1 as proposed by Ruan et all [10]. For this aim, following 3 measurements ( at 5,6 and 7 cm locations) were anticipated first, and eliminated after calculation. There are 8 values including three anticipations for the solution. The resultant equation becomes

$$I(p, j) = \sum_{l=0}^7 a_0^l J_0(I_0^{l+1} r) L \quad (5)$$

Where  $L$  is calculated for each observation (integration) path separately and it is independent summation which comes into the equation as a constant. For each observation path, an  $8 \times 8$   $a_0^l$  matrix is created and by matrix calculation those coefficients are determined to generate a general formula. Before this matrix calculation is applied, a smoothing function (using Savitzky-Golay smoothing.) was applied to experimentally obtained data to get rid out of experimental errors. The coefficients and final response is modeled by matrix applications.

### 3. Experimental Setup

The experiments are carried out in a specially designed Confined-CCP (27.12 MHz) discharge system. Figure 2 shows the schematic of C-CCP and MWI measurements system. The system consists of two parallel-plate electrodes of equal area, with a diameter of 140 mm, which are separated by a 50 mm gap. Gas is pumped into the discharge region through a 'showerhead' in the grounded electrode. The discharge is confined between the electrodes using a cylindrical quartz tube (wall thickness of 5 mm). The quartz tube window both shields the discharge from the grounded chamber walls and creates a pressure differential between the inside and outside of the tube. Therefore the discharge exists inside the quartz tube, but outside the tube the pressure is too low for plasma discharge. A low power 20mW microwave signal from a swept YIG voltage controlled oscillator was coupled into the reactor through a sidewall via an X band waveguide and its horn antenna. The antenna orientation was such that the electric-field direction of the microwave beam is perpendicular to the electric field between the plasma electrodes.

Horn antennas are placed such that both transmitter and receiver antennas are aligned at the mid plane between the two electrodes. Antenna distances from the centre line, drawn dashed at figure2, are variable in the  $z$  direction which allows us collecting seven data points for each pressure and each power level up to 4 cm away from the center line. Since there is no line of sight observation path at the edge of reactor, zero number of electron density have been assumed. By the same manner, number density at 5cm, 6cm and 7cm from the centre line have also been anticipated based on the experimental results. Since the wavelength of the interferometer is about  $\approx 1.96$ cm, its resolution does not allow making measurement by 1cm resolution. But, axially moving receiving system can predict a data for a certain position by  $\approx \pm 1$ cm which means that half of obtained data is overlapped with half of previous/next position. Resultant data representation includes moving average techniques with a certain error. Electrodes are driven by 27.12 MHz while RF output power varies between 20 Watts to 500 Watts, at three different plasma pressures.

The YIG oscillator is swept from 15.300 GHz to 15.330 GHz with a triangle ramp signal. There is 7 meters difference between reference and plasma leg. This frequency difference results in an increase in the path difference of one additional wavelength. The output from the square-law detector approximates a sinusoid over the  $2\pi$  phase change which occurs during the frequency sweep. With no plasma, the phase of the zero crossing of the signal to the phase of the reset of the triangle-ramp is noted and defined as zero phases.

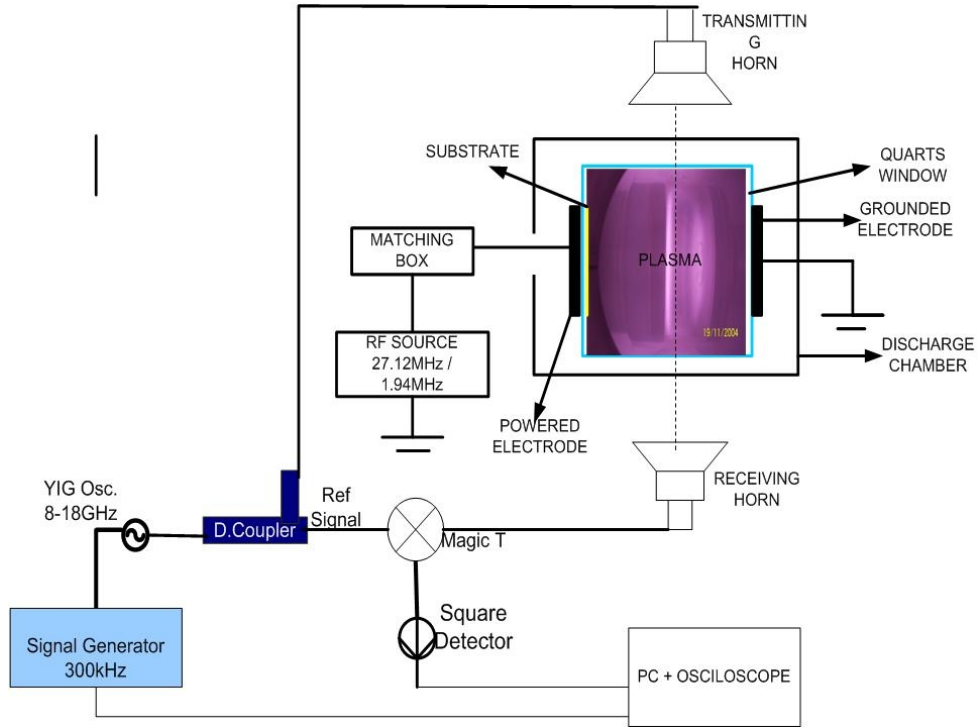


Fig.2. Schematic of Interferometer.

#### 4. Experimental Results and Discussion

Microwave interferometer measurements are taken at 5 Pa, 15 Pa and 30 Pa with a variable RF power source to investigate density profile. In figure 3 line-integrated plasma densities at the center of the discharge are given as a function of RF power. Density increases linearly with RF power in agreement with global modeling. As the power increases, error in the measured electron number density increases from  $\pm 17\%$  to  $\pm 25\%$ .

Figure 4 represents a radial electron density distribution (the result of Abel inversion) at 5 Pa for power levels of 10 W, 20 W, 40 W, 160 W, 320 W, and 500 W. Electron density distribution has a maximum at the center and decreases to a minimum at the boundary for the power levels of 10 W and 20 W. This behavior is similar to pre-sheath like behavior in weakly collisional plasma [13]. Ions also diffuse to the boundaries due to the density gradient and the capacitive discharges should be modeled two dimensional. Number density on center line is about 10 times higher than the edge of the electrodes for these power levels. Measured center plasma electron densities are  $3.71 \times 10^{14} \text{ #/m}^3$ ,  $9.5 \times 10^{14} \text{ #/m}^3$  for 10 W and 20 W respectively. By 160 W of applied power second peak appears at 3 cm away from the centre line which increases with respect to applied power, and it becomes  $\approx 75\%$  larger than the centre line density. While the centre line density is  $1.25 \times 10^{16} \text{ #/m}^3$ ,  $1.20 \times 10^{16} \text{ #/m}^3$  and  $5.34 \times 10^{15} \text{ #/m}^3$  for 500 W, 320 W and 160 W, respectively, their second peaks reach the values of  $2.01 \times 10^{16} \text{ #/m}^3$ ,  $1.7 \times 10^{16} \text{ #/m}^3$  and  $5.01 \times 10^{15} \text{ #/m}^3$ . Electron number density at each radial position increases monotonically, with the same axial density profile in each case [14]. The central  $\sim 4$  cm have a cosine density profile as expected for uniform ionization rate, and the outer 5 cm show decreasing density as the

radial boundary condition becomes a significant loss surface once the radial boundary is within the distance of the electrode separation.

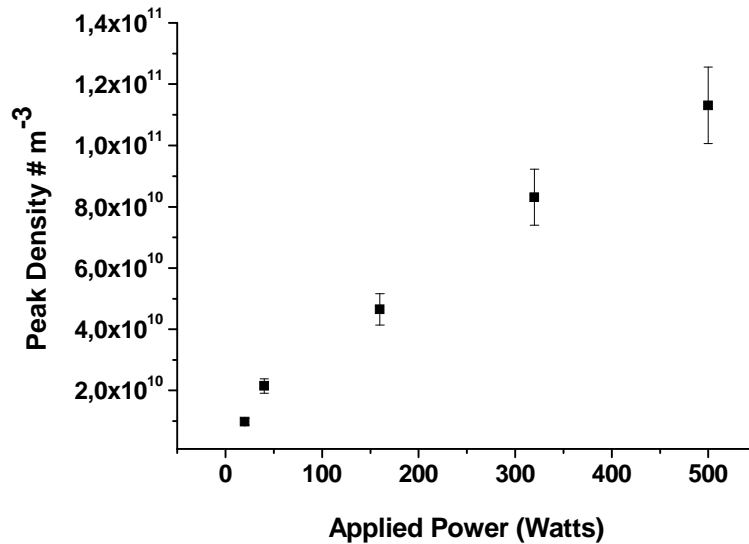


Fig. 3. Line-integrated plasma densities at the center of the discharge vs. RF power.

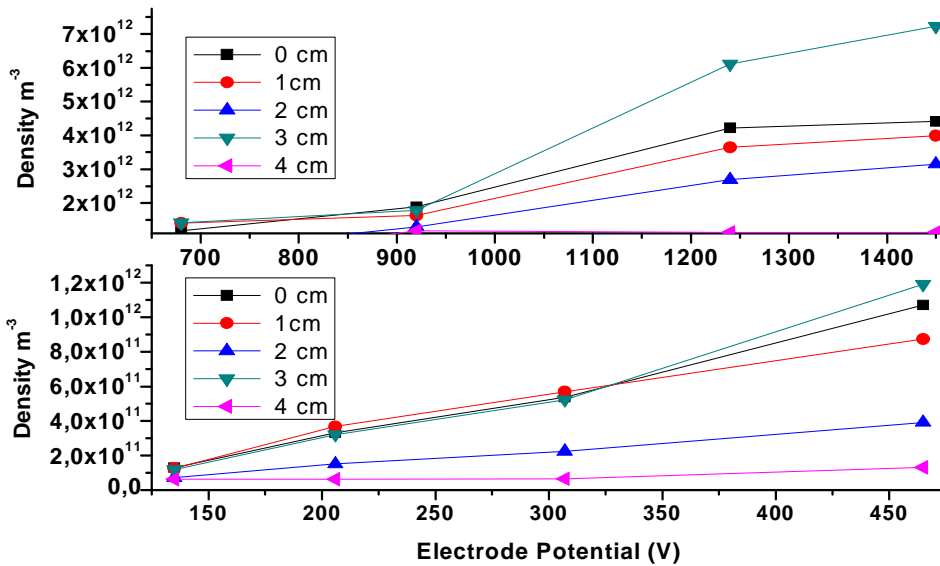


Fig. 4. Radial Electron Density Distribution depending on electrode voltage at 37.5mTorr

Figure 5 represents radial electron number density distribution for 500 W, 320 W, 160 W, 80 W, 40 W, 20 W, 10 W and 5W of driving single power output at 15pascal pressure level. Same responses are obtained as 5Pa so that at this pressure regime, electron number density is

about 65% less than the 5 Pascal in this regime. This case, second peak reaches the central peak density by 80 W of applied power. Similarly plasma density at the center point and second peak (at 3cm) is about 6 times higher than 1 cm from electrode edges for all power levels.

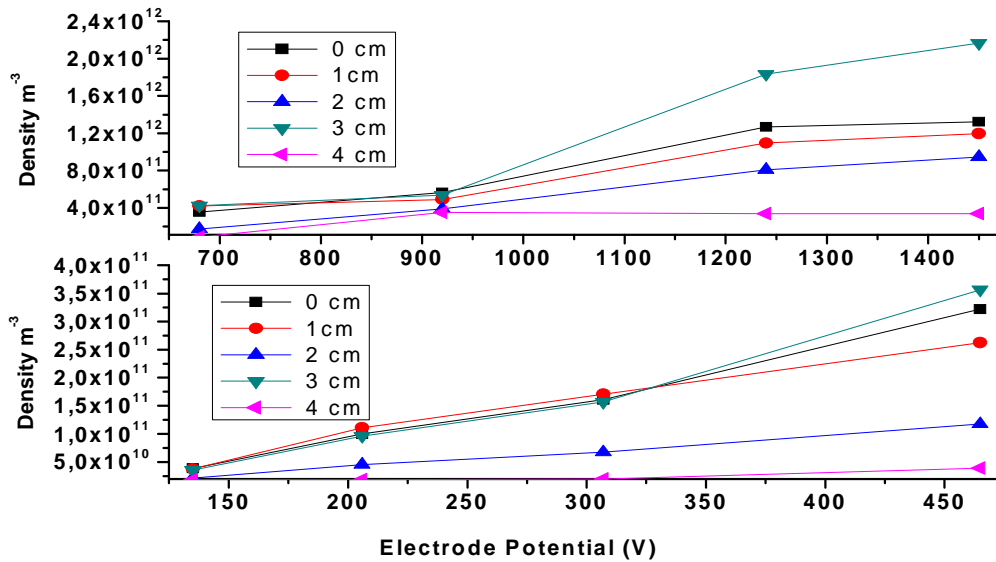


Fig. 5. Radial Electron Density Distribution depending on RF output power at 100mTorr.

Figure 6 represents an axial electron density distribution at 30 Pa for power levels of 500 W, 320 W, 160 W, 40 W, 20 W and 10 W at 30 Pascal. In this pressure regime, second peak becomes about 10% bigger than central density by 40 W of applied power. Maximum density of second peak of 40 W is  $1.04 \times 10^{15}$  at second peak location. Compared to 5 Pa results, electron number density is about 70% less. Note that the electron number density at 1cm from the electrode edges is about five times less than the center line number density.

Figure 7 presents the axial electron density profile for single frequency application at three different frequency regimes. 500 Watt of power is supplied to the driving electrode at 27.12 MHz. As expected, ne density decreases as the pressure increases from 5 Pa to 15 Pa dramatically and continues to decrease up to 30 Pa. At each power level, electron number density variation from centre lines to the radial boundary track each other. They have similar shape, which will be interpreted as the pre-sheath shape dependent on weakly collisional plasma. It is seen from two plots that, for low power such as 20 W, second peak (at 3cm location) is less than central density as well as it is about 10 to 20% bigger than central density for high power levels such as 500 W.

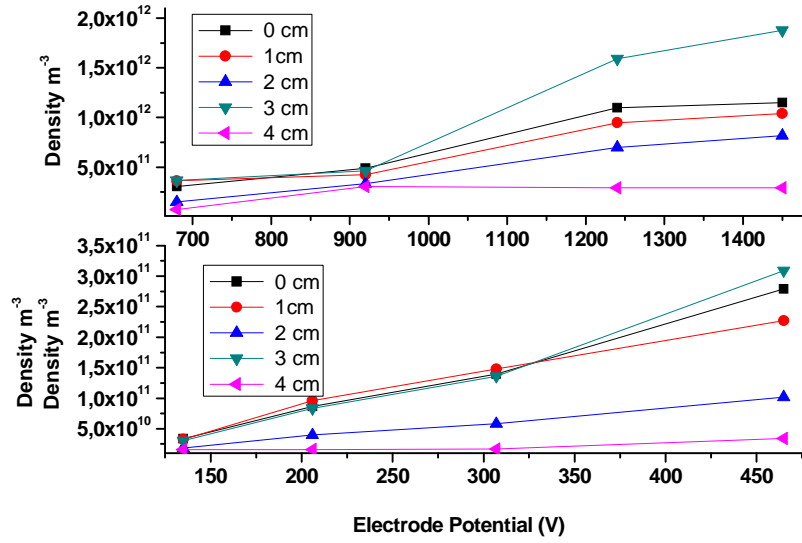


Fig. 6. Radial Electron Density Distribution depending on RF output power at 200mTorr.

Plasma density decreases as the pressure increases from 5 Pa to 30 Pa. Assuming Boltzmann electrons, the electron density can be written as a function of potential as in equation 6 [15].

$$n_e(y) = n_0 e^{\frac{ej(y)}{T_e}} \tag{6}$$

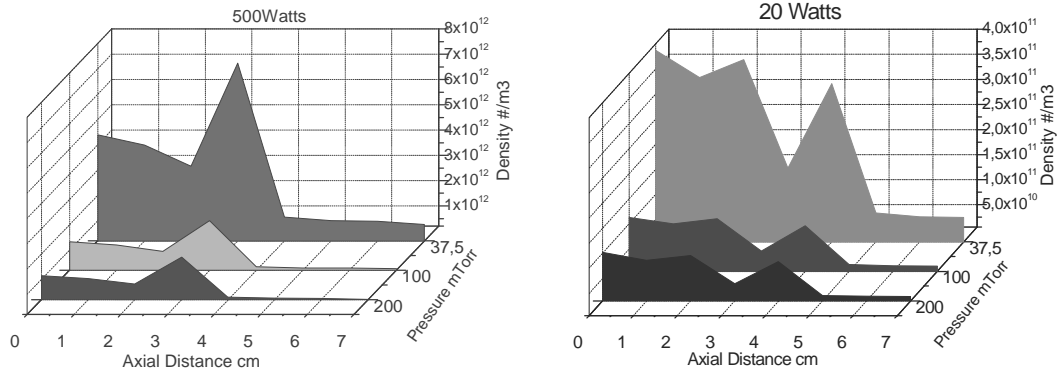


Fig. 7. Axial density profiles for different pressures.

From Equation 6 the normalized potential with respect to electron temperature can be pulling out and axial potential profile can be obtained. The axial potential profile for 20 Watts at 5 Pa is given in figure 8. But for higher power levels, same response cannot be obtained. The potential drop from center to the boundary edge is approximately two electron temperature [16,17,18].

While the ions diffuse to the main electrodes there are diffusion losses to the side boundaries usually neglected in modeling of capacitive discharges.

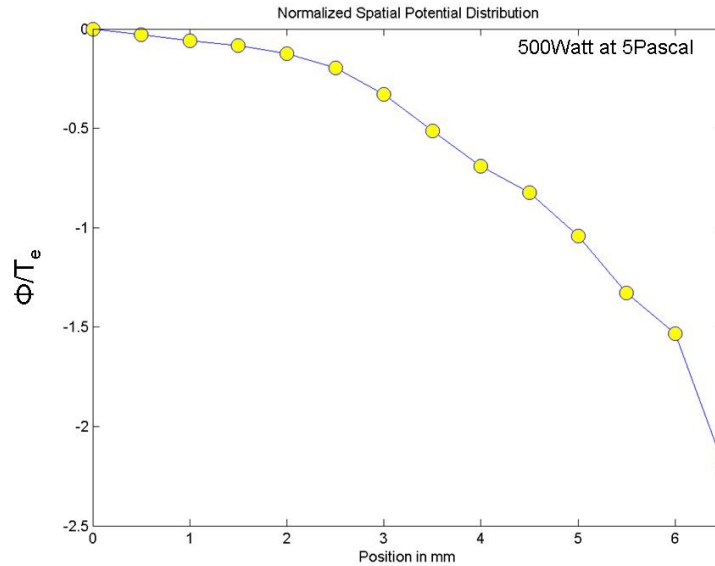


Fig. 8. Normalized plasma potential distributions

Figure 9 shows the plasma density profile with respect to power at different pressures. Note that the plasma density goes up as the pressure decreases from 30 Pa to 5 Pa. This increase is a result of the stochastic heating mechanism at lower pressures [19].

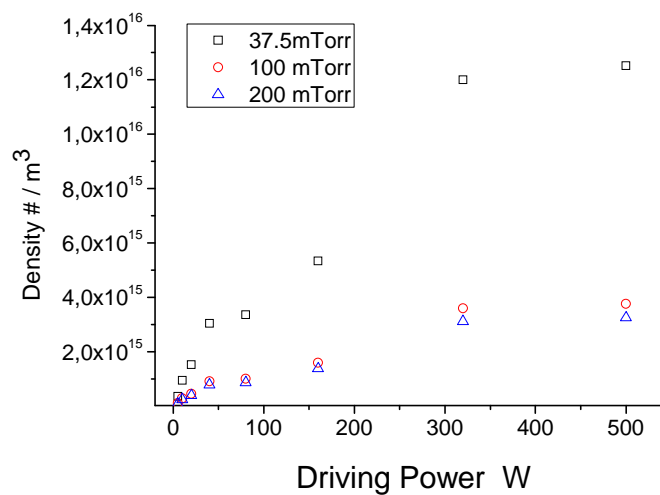


Fig. 9 .Center plasma density variations with respect to power for different pressures.

## 5. Conclusion

The plasma electron density in a quartz tube confined capacitively coupled hydrogen plasma discharge system, is measured axially using microwave interferometer method with Abel inversion technique for different powers and pressures. The normalized potential profile is obtained with the assumption of the Boltzmann electrons indicates that the potential drop is almost two electron temperature from center to the boundary which is neglected usually CCP modeling. The density increases as the pressure decreases. This is a result of stochastic heating mechanism that is dominant at low pressures. As the power increases the density increases linearly. This behavior confirms the global modeling of power dependence for CCP [20]

**Acknowledgement:** I would like to thank to ATRP and Euratom for hosting my stay in Dublin. This work has been accrued at Plasma Research Laboratory, School of Physical Sciences and National Centre for Plasma Science and Technology, DCU- Ireland. I also would like to thank to Mr. Cezar Caman for his kind full helping about mass spectrometer data collection and analysis.

## References

- 
- [1] Makoto Sekine, Study for Plasma Etching of dielectric film in semiconductor device manufacturing. Review of ASET Project, Pure Appl. Chem., V: 74, No:3, pp. 381–395, 2002.
  - [2] Y.J. Lee, K.N. Kim, B.K. Song, G.Y. Yeom, Internal linear inductively coupled plasma (ICP) sources for large area FPD etch process applications, Materials Science in Semiconductor Processing 5 (2003) 419–423.
  - [3] E. Kır , L. Oksuz, S. Helhel, Preparation of Poly(2-chloroaniline) Membrane and Plasma Surface Modification, Applied Surface Science, xxx (2005) xxxx, Received 26 February 2005, Accepted 18 May 2005 - APSUSC 12915 1-6 (In Press).
  - [4] B. Chapman, Glow Discharge Processes, Wiley, New York, (1980)
  - [5] J.C. Cecci, Lecture Notes for the course ‘Production and Diagnostic of Process plasma’, (Princeton Scientific Consultant, Inc, NJ, November 1984.
  - [6] B.E. Gilchrist, S.G. Ohler, A.D. Gallimore, Flexible microwave System to measure the electron number density and quantify the communications impact of the electric thruster plumes, Rev. Sci. Instruments, 68(2) February (1997).
  - [7] Xiao Feng Ma, Tatsuoki Takeda, Asymmetric Abel Inversion by Neural network for reconstruction of plasma density distribution, Nuclear Instruments and Methods in Physics Research, A 492 178-189 (2002).
  - [8] P. Tomassini, A. Giuliatti, A generalization of Abel inversion to non-axisymmetric density distribution, Optics Communication, 199 143-148 (2001).
  - [9] M. J. Buie, J. T. P. Pender, J. P. Hollowat, T. Vincent, P. L. G. Ventzek, and M. L. Brake, Abel’s Inversion Applied to Experimental Spectroscopic Data with off Axis Peaks, J. Quant. Spaw. Radiat. Transfer Vol. 55, No. 2, pp. Z-243, (1996).
  - [10] Hualin Ruan, Boanian Wan, A new Method for Asymmetrical Inversion Using Fourier-Bessel Expansions, International Journal of Infrared and Millimeter Waves, Vol.21 No:12 (2000).

- 
- [11] Ch Lukas, M Muller, V Schulz-von der Gathen and H F Dobele, Axially resolved electron density distribution in an RF excited parallel plate plasma reactor by 1 mm MWI, Plasma Sources Sci. Technol. 8 94–99. Printed in the UK (1999).
  - [12] S. Helhel, L. Oksuz, B. Ellingboe and C. Gaman, Plasma Density Measurements of Confined Capacitively Coupled Plasma by Microwave Interferometer and Ion Energy Distribution Function Methods, Plasma Sources Science and Technology, (Submitted at February 22, 2005, Reference No. NH0855).
  - [13] K.U. Riemann, Phys. Fluids B 4, 2693 (1992)
  - [14] J. Koo, N.Y. Babaeva, H.C. Kim, O.V. Manuilenko and J.W. Shon, Simulation of Capacitively Coupled Single and Dual Frequency RF Discharges, IEEE Transactions on Plasma Science, Vol 32, No:1, pp.47-53, February 2004.
  - [15] Francis F. Chen, Introduction to Plasma Physics and Controlled Fusion, Second Edition, pp:75, 1984 Plenum Press, NY&London.
  - [16] L. Oksuz and N Hershkowitz PRL, 89(14):art.no.145001 September 30 (2002).
  - [17] L. Oksuz and N. Hershkowitz Plasma Sources Sci. and Tech. Vol 14 No 1 p 201 (2005)
  - [18] Oksuz L. and Hershkowitz N. Plasma Sources Sci. and Tech. 13 263-271 (2004).
  - [19] Deborah O'Connell, Investigations of high voltage plasma boundary sheaths in radio-frequency discharges operated with multiple frequencies, Ph.D. Thesis, Dublin City University, School of Physics – PRL, 13th July 2004.
  - [20] Michael A. Lieberman and Allan J. Lichtenberg, principles of Plasma discharges and Material processing, John Wiley and Sons Inc, 1994.